frontiers | Frontiers in Chemistry

TYPE Original Research
PUBLISHED 06 August 2024
DOI 10.3389/fchem.2024.1358353

OPEN ACCESS

EDITED BY
Hyunook Kim,
University of Seoul, Republic of Korea

REVIEWED BY
Lakshmi Narayanan Mosur Saravana Murthy,
Intel, United States
Gayani Pathiraja,
University of North Carolina at Greensboro, United States

*CORRESPONDENCE
Farid A. Harraz,
faharraz@nu.edu.sa
Mohammed M. Rahman,
mmrahman@kau.edu.sa

RECEIVED 19 December 2023
ACCEPTED 26 June 2024
PUBLISHED 06 August 2024

CITATION
Faisal M, Alam MM, Ahmed J, Asiri AM, Algethami JS, Altholami RH, Harraz FA and Rahman MM (2024), Efficient nitrite determination by electrochemical approach in liquid phase with ultrasonically prepared gold-nanoparticle-conjugated conducting polymer nanocomposites.
Front. Chem. 12:1358353.
doi: 10.3389/fchem.2024.1358353

Efficient nitrite determination by electrochemical approach in liquid phase with ultrasonically prepared gold-nanoparticle-conjugated conducting polymer nanocomposites

M. Faisal[1,2], M. M. Alam[3], Jahir Ahmed[1,2], Abdullah M. Asiri[4,5], Jari S. Algethami[1,2], Raed H. Altholami[6], Farid A. Harraz[1,7]* and Mohammed M. Rahman[4,5]*

[1]Promising Centre for Sensors and Electronic Devices (PCSED), Advanced Materials and Nano-Research Centre, Najran University, Najran, Saudi Arabia, [2]Department of Chemistry, Faculty of Science and Arts, Najran University, Najran, Saudi Arabia, [3]Department of Chemical Engineering, Faculty of Engineering and Technology, Z. H. Sikder University of Science and Technology (ZHSUST), Shariatpur, Bangladesh, [4]Center of Excellence for Advanced Materials Research (CEAMR), King Abdulaziz University, Jeddah, Saudi Arabia, [5]Department of Chemistry, Faculty of Science, King Abdulaziz University, Jeddah, Saudi Arabia, [6]Department of Chemistry, College of Art and Science, Prince Sattam bin Abdulaziz University, Wadi Al Dawasir, Saudi Arabia, [7]Department of Chemistry, Faculty of Science and Arts at Sharurah, Najran University, Sharurah, Saudi Arabia

An electrochemical nitrite sensor probe is introduced herein using a modified flat glassy carbon electrode (GCE) and $SrTiO_3$ material doped with spherical-shaped gold nanoparticles (Au-NPs) and polypyrrole carbon (PPyC) at a pH of 7.0 in a phosphate buffer solution. The nanocomposites (NCs) containing Au-NPs, PPyC, and $SrTiO_3$ were synthesized by ultrasonication, and their properties were thoroughly characterized through structural, elemental, optical, and morphological analyses with various conventional spectroscopic methods, such as field-emission scanning electron microscopy, energy-dispersive X-ray spectroscopy, high-resolution transmission electron microscopy, powder X-ray diffraction, X-ray photoelectron spectroscopy, and Brunauer–Emmett–Teller method. The peak currents due to nitrite oxidation were characterized in detail and analyzed using conventional cyclic voltammetry (CV) as well as differential pulse voltammetry (DPV) under ambient conditions. The sensor response increased significantly from 0.15 to 1.5 mM of nitrite ions, and the sensor was fabricated by coating a conducting agent (PEDOT:PSS) on the GCE to obtain the Au-NPs/PPyC/$SrTiO_3$ NCs/PEDOT:PSS/GCE probe. The sensor's sensitivity was determined as 0.5 μA/μM•cm^2 from the ratio of the slope of the linear detection range by considering the active surface area (0.0316 cm^2) of the flat GCE. In addition, the limit of detection was determined as 20.00 ± 1.00 μM, which was found to be satisfactory. The sensor's stability, pH optimization, and reliability were also evaluated in these analyses. Overall, the sensor results were found to be satisfactory. Real environmental samples were then analyzed to evaluate the sensor's reliability through DPV, and the results showed that the proposed novel electrochemical sensor holds great

promise for mitigating water contamination in the real samples with the lab-made Au-NPs/PPyC/$SrTiO_3$ NC. Thus, this study provides valuable insights for improving sensors for broad environmental monitoring applications using the electrochemical approach.

KEYWORDS

Au-NPs/PPyC/SrTiO3 nanocomposites, nitrite detection, glassy carbon electrode, differential pulse voltammetry, environmental remediation

Introduction

Nitrates (NO_3^-) and nitrites (NO_2^-) are chemical compounds that are generally used as food preservatives in processed meats, such as bacon, ham, sausages, and hot dogs. They inhibit the growth of bacteria, particularly *Clostridium botulinum*, which is responsible for causing botulism. These nitrates and nitrites also contribute to the characteristic flavor, color, and aroma of cured and processed meats (Kalaycıoğlu and Erim, 2019; Karwowska and Kononiuk, 2020); moreover, they have been known for their potential to form nitrosamines in the stomach, particularly amines and amino acids. Nitrosamines are considered as carcinogens that cause various cancers, including stomach, esophageal, colorectal, and pancreatic cancers (Bartsch et al., 1989; Nawrocki and Andrzejewski, 2011). Nitrates and nitrites can also be converted into nitric oxide (NO) in the human body through various biological processes; nitric oxide plays a positive role in immune function and neurotransmission. Additionally, nitrates and nitrites are naturally present in foods, such as vegetables, fruits, grains, and water, and these dietary nitrates are generally considered safe for health benefits, such as cardiovascular health support and reduced risk of certain diseases (Bahadoran et al., 2016; Bedale et al., 2016; Huang et al., 2022). However, nitrates can leach into the groundwater and surface water when excess nitrogen-based fertilizers are used in agriculture or when sewage and animal wastes are improperly managed. Elevated nitrate levels in drinking water can pose health risks, particularly for infants and young children, as excessive nitrate consumption can lead to a condition known as methemoglobinemia (or blue baby syndrome), which interferes with the ability of the blood to carry oxygen (Tamaki et al., 2003; Meng et al., 2009; Lu et al., 2023). Thus, to develop a system to monitor nitrite contamination in the environment and concentrations in bodily fluids (blood and urine), a reliable sensor is necessary.

Accordingly, procedures involving chromatography (Hamilton and Lewis, 2006), Fourier-transform infrared (FT-IR) spectrometry (Griffiths and De-Haseth, 2007), laser absorption spectroscopy (LAS) (Edwards et al., 2003), and optical analyses (Hassan et al., 2022; Kang et al., 2023) have been implemented to measure nitrite levels in real samples. However, these techniques are unreliable owing to their poor sensitivities, narrow detection ranges, longer analysis times, higher costs, and lower portabilities. To overcome these problems, researchers are working hard to develop alternative techniques. As a result, voltammetric techniques like differential pulse voltammetry (DPV) and cyclic voltammetry (CV) have become popular detection approaches. In recent years, some reports have claimed that working electrodes made of graphite, glassy carbon, carbon paste, and other noble metals could be successfully applied to detect unknown concentrations of nitrites using voltammetric electrochemical approaches (Kaminskay et al., 2004). However, pure-metal electrodes are limited by poor electron transport and selective electrode surfaces. Alternatively, as reported elsewhere, the functioning electrode surfaces are modified with sensing substrates to develop electrochemical sensors (Terbouche et al., 2016; Tohidinia et al., 2018; Amini et al., 2021; Wang C. et al., 2024).

Amperometry and DPV are commonly used electrochemical methods for detecting trace amounts of toxic contaminants. In this study, the general and reliable voltammetric method was used to develop a nitrite electrochemical sensor. Accurate nitrite detection in aqueous systems, metal composites, metal oxides, and organometallic substances like zinc oxide nanoflowers and reduced graphene oxide (RGO), tin dioxide nanoparticle/RGO hybrids, graphene/polymer nanofibers, and nanocomposites of conducting polymers are well documented. Hence, the present study aimed to develop an electrochemical sensor probe using conductive PEDOT: PSS polymer composited with a sensing layer via metals and metal oxides for reliable electrochemical determination of nitrites to detect trace levels of the target analytes; this would also ensure environmental and health safety in a broad scale. Gold nanoparticles (Au-NPs) and $SrTiO_3$ have gained significant attention in various fields owing to their unique optical, electronic, and catalytic properties. In nitrite sensing, Au-NPs are utilized for their ability to detect nitrite ions (NO_2^-) based on electrochemical changes or electrocatalytic sensing mechanisms. The roles of the Au-NPs in nitrite sensing include amplification of the sensing signal due to their high surface-area-to-volume ratio and excellent catalytic properties. These properties enhance the sensitivity of the nitrite sensor, allowing the detection of low concentrations of nitrite ions in samples. Moreover, $SrTiO_3$ is a semiconductor material with a wide bandgap; its electronic properties can be modified by doping or surface functionalization, making it suitable for sensing applications. When exposed to nitrite ions, $SrTiO_3$ undergoes changes in its electrical conductivity or surface potential, which can be used for sensing purposes. The surfaces can be engineered to exhibit high reactivity toward nitrite ions. Functionalization of the $SrTiO_3$ surface with specific molecules or ions enhances its selectivity toward nitrite ions, enabling detection of nitrites in complex sample matrices. This plays a crucial role in nitrite sensing by providing a platform with tunable electronic properties, high reactivity toward nitrite ions, and compatibility with sensing devices, enabling the development of robust and sensitive nitrite sensors for various applications involving environmental monitoring, food safety, and biomedical diagnostics. The significant roles of Au-NPs in nitrite sensing also involve serving as transducers, signal amplifiers, and platforms for selective

detection, thereby enabling the development of sensitive, selective, and reliable nitrite sensors for various applications involving environmental monitoring, food safety, and healthcare.

Herein, we report the development of Au-NPs/PPyC/$SrTiO_3$ nanocomposites (NCs) using ultrasonic techniques and utilization of these nanostructures for electrochemical sensing of nitrites in a buffer of 7.0 pH. To date, numerous NCs of polypyrrole (PPy) have been used to develop electrochemical sensors, such as humidity (Hussain et al., 2021), serotonin (Song et al., 2019), NH_3 (Kharat et al., 2007), and DNA (Booth et al., 2011) sensors. In addition, many reliable nitrite electrochemical sensors have been fabricated to detect gaseous nitrites by applying PPy films (Navale et al., 2014a), PPy-WO_3 CNs (carbon nanostructure) (Mane et al., 2015), CSA (Camphor sulfonic acid)-PPy (Navale et al., 2014b), Ag-PPy NCs (Karmakar et al., 2017; Zhang et al., 2024), and PPy/N-Multiwall Carbon Nanotube (MWCNT) (Liu et al., 2019). To the best of our knowledge and a literature survey, there are no available studies on this topic; thus, the present study involves development of Au-NPs/PPyC/$SrTiO_3$ NCs embedded with PEDOT:PSS/glassy carbon electrode (GCE) and utilized for the first time in an electrochemical approach.

Experimental

Materials and methods

To prepare the hybrid NC materials, a block copolymer with a molecular weight of 12,600 g/mol, F127 surfactant, titanium (IV) butoxide (TBOT), zinc acetate, polypyrrole-doped carbon (PPyC), $HAuCl_4{\cdot}4H_2O$, methylene blue, hydrochloric acid, acetic acid, ethanol, and methanol were utilized. All chemicals were purchased from Sigma-Aldrich and used as received without further purification.

Preparation of $SrTiO_3$

To prepare $SrTiO_3$, pluronic F127 (2.4 g) was first dissolved in ethanol (30.0 mL). A mixture of 3.5 mL of TBOT, 0.74 mL of 35% hydrochloric acid, and 2.3 mL of acetic acid was added to this solution in a conical flask and stirred constantly at room temperature for an hour. Subsequently, approximately 2.23 g of $Sr(NO_3)_2$ was added to the mixture to form a mesophase of CH_3COOH-TBOT-F127 using Sr:Ti in the molar ratio of 1:1. This solution was stirred continuously for 60 min, and the ethanol was evaporated by drying the resulting solution at 40°C and 40% humidity for 24 h. Finally, the gel slurry was aged at 65°C and heated at the rate of 1°C per minute for 4 h at 900°C in a muffle furnace to obtain the mesoporous $SrTiO_3$ material.

Synthesis of the Au-NPs/PPyC/$SrTiO_3$ NC

Next, the 10% PPyC/$SrTiO_3$ NC was prepared by the ultrasonication method. $SrTiO_3$ (1.0 g) and PPy (0.1 g) were ultrasonicated in 100.0 mL of deionized (DI) water for 15 min, filtered carefully, and then washed with ethanol and DI water. Over the next 24 h, the wet precipitate was dried at 65.0°C, resulting in the formation of the 10% PPyC/$SrTiO_3$ NC. To create a ternary framework, 1% Au-NPs was added to the NC using the photoreduction strategy, as reported previously (Faisal et al., 2022; Li Q. et al., 2023; Wang S. et al., 2024). A solution of $HAuCl_4{\cdot}4H_2O$ (1% Au) was added dropwise to 0.5 g of the 10% PPy/$SrTiO_3$ suspension in 100 mL of DI water, and the suspension was placed under a mercury lamp (2.0 mW/cm^2) for 12 h with continuous stirring. The resulting mixture was centrifuged 3–4 times violently for appropriate separation of the desired material. Thereafter, the obtained material washed with ethanol and DI water before being dried at 65°C for 24 h to obtain the final product: Au-NPs/PPyC/$SrTiO_3$ NC.

Characterization of the Au-NPs/PPyC/$SrTiO_3$ NC

The prepared NCs were thoroughly characterized for functional, morphological, structural, elemental, and surface area analyses using conventional testing methods. The structural and crystalline properties of the Au-NPs/PPyC/$SrTiO_3$ NC were analyzed by various techniques. A PANalytical (X'port) diffractometer was used for the powder X-ray diffraction (XRD) analysis with Cu $K_{1/2}$ (1 = 154.060, 2 = 154.439 p.m.) radiation. The NC was then analyzed by field-emission electron microscopy (FESEM; JEOL-6300F) and high-resolution transmission electron microscopy (HRTEM; JEOL JEM-2100F-UHR) at 200 kV attached to a 1k charge coupled device (CCD) camera and a Gatan energy filter (GIF, 2001) to determine the morphology and structure. The binding energy of the Au-NPs/PPyC/$SrTiO_3$ NC was determined by X-ray photoelectron spectroscopy (XPS) using a VGESCALAB 200R P Thermo VG system equipped with a hemispherical electron analyzer and MgKα radiation (hν = 1253.6 eV). The Brunauer–Emmett–Teller (BET) surface area and pores size variation were analyzed at 77 K on a Quantachrome: NOVA 4200 analyzer with overnight degassing at 200.0°C. We then analyzed the Halsey-equation-based adsorption data using the Barrett–Joyner–Halenda (BJH) model and also determined the BET surface area. Additionally, diffuse reflectance spectra collected between 200 and 800 nm were used for the bandgap energy study employing a Shimadzu UV-Vis 3600 spectrophotometer; the results were collected for each freshly generated NC sample.

Development of the glassy carbon working electrode

A GCE was modified using the Au-NPs/PPyC/$SrTiO_3$ NC to create the working electrode (WE) of the sensor. This was achieved by preparing a NC-ethanol slurry, and the GCE's flat surface was covered with a thin coating of the slurry before being air-dried in open air. About 10.0 µg of PEDOT:PSS (in a 5% ethanol solution) was added to maintain the strength of the GCE's deposited layer. The modified GCE was then heated at 35°C for an hour. The desired electrochemical sensor was assembled using a potentiostat of Metrohm Autolab modules with the modified GCE as the WE, Ag/AgCl (saturated KCl) as the reference electrode, and Pt wire as

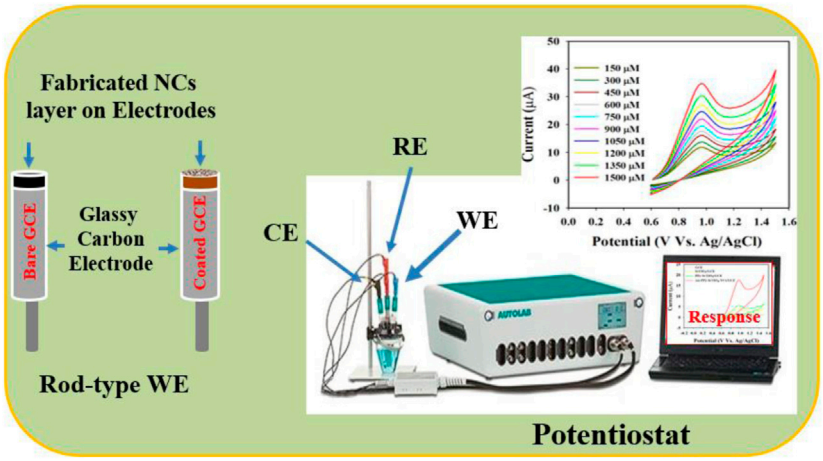

FIGURE 1
Schematic representation of the fabricated nitrite sensor probe with a modified glassy carbon electrode (GCE) and Auto-Lab assembly operation.

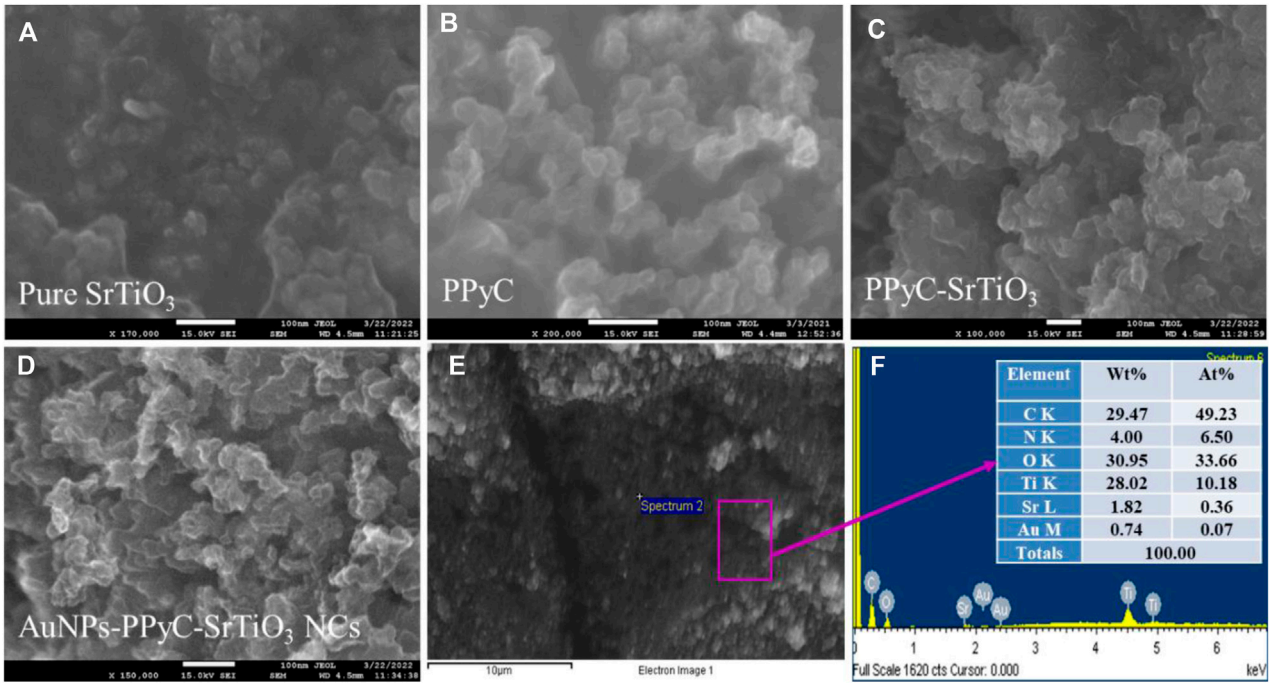

FIGURE 2
FESEM and EDS analyses of the nanocomposites (NCs). Magnified images of the **(A)** pure $SrTiO_3$, **(B)** PPyC, **(C)**/PPyC/$SrTiO_3$, and **(D)** Au-NPs/PPyC/$SrTiO_3$ NCs; **(E)** EDS image of the Au-NPs/PPyC/$SrTiO_3$ NC and **(F)** elemental composition of Au-NPs/PPyC/$SrTiO_3$ NC.

the counter electrode, as shown in Figure 1. The electrochemical investigations were carried out via CV by diluting the nitrite in a phosphate buffer saline (PBS) medium at pH 7, with the concentrations ranging from 0.15 to 1.5 mM. The obtained data were then used to determine the sensor's sensitivity, limit of detection (LOD), linear detection range (LDR), stability, and effect of pH during analysis of the fabricated material. The LOD was obtained from the equation LOD = 3.3σ/S, where σ and S refer to the standard deviation of the blank responses and slope of the calibration curve, respectively.

Results and discussion

FESEM and EDS analysis of Au-NPs/PPyC/$SrTiO_3$ nanocomposites

The structural and morphological properties of the newly created Au-NPs/PPyC/$SrTiO_3$ NCs and its constituent elements were analyzed by FESEM to obtain high-resolution images exhibiting the size, shape, and morphology. FESEM coupled with EDS was used to study the elemental composition of the NC.

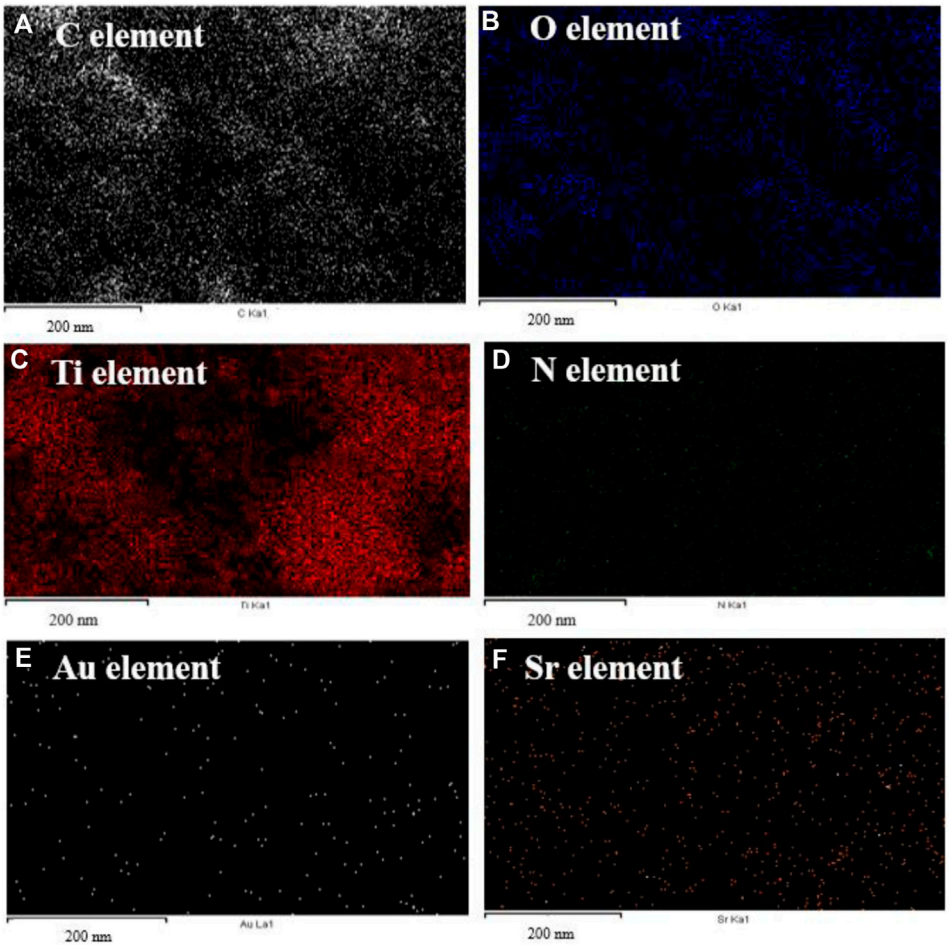

FIGURE 3
EDS mapping for elemental distribution in the Au-NPs/PPyC/$SrTiO_3$ NC: **(A)** C, **(B)** O, **(C)** Ti, **(D)** N, **(E)** Au, and **(F)** Sr.

Figure 2 shows the FESEM and EDS images of the NC at high magnifications. As shown in Figure 2, the $SrTiO_3$ particles exhibit irregular spherical shapes intercalated with PPy and Au-NPs. However, the prepared Au-NPs/PPyC/$SrTiO_3$ NCs did not show any particular shapes or sizes at the nano level, as seen in the FESEM images in Figures 2A–C, and Figure 2D indicates that these are NCs. Similar observations can be made from Figure 2E for the elements. Elemental analysis of the Au-NPs/PPyC/$SrTiO_3$ NCs using EDS revealed that they were composed of C (29.47%), O (30.95%), Ti (28.02%), Sr (1.82%), N (4.00%), and Au (0.74%), as seen in Figure 2F. Thus, EDS analysis confirmed the existence of Au, C, O, Ti, N, and Sr in the synthesized NCs.

Elemental mapping of the Au-NPs/PPyC/$SrTiO_3$ NCs involves spatially resolved analysis of the distribution of each element within the NC structure. This technique provides valuable insights into the composition, morphology, and distribution of the constituents of the Au-NPs/PPyC/$SrTiO_3$ NC. The spatial distribution of each element in the NC is shown in Figure 3. Each pixel/color dot in the map represents a specific area of the target sample, and the intensity of the pixel/dot corresponds to the concentration of the element detected in the prepared Au-NPs/PPyC/$SrTiO_3$ NC. Additionally, by analyzing the elemental mapping, we can identify regions rich in specific elements and assess the uniformity or segregation of different components within the Au-NPs/PPyC/$SrTiO_3$ NC. Here, the elemental mapping of each element was obtained separately, as presented in Figure 3. These maps are analyzed to gain insights into the composition and distribution of the NC constituents, which are analyzed and presented for C in Figure 3A, O in Figure 3B, Ti in Figure 3C, N in Figure 3D, Au in Figure 3E, and Sr in Figure 3F. Thus, EDS mapping confirmed the existence and dispersion of Au, C, O, Ti, N, and Sr in the synthesized Au-NPs/PPyC/$SrTiO_3$ NCs.

HRTEM analysis of the Au-NPs/PPyC/$SrTiO_3$ NC

In this analysis, spherical-shaped nanoparticles ranging in size from 100.0 nm to 300.0 nm were found in the Au-NPs/PPyC/$SrTiO_3$ NC, while the PPy polymer crystallized into a network of compact particle-shaped nanostructures. Figures 4A–C and Figure 4D demonstrate the findings of the HRTEM study, which validates the morphological structures of the Au-NPs, PPyC, and $SrTiO_3$ separately. PPy is shown to be intercalated with $SrTiO_3$ and Au-NPs in the HRTEM images. Figures 4E, F display the HRTEM and diffraction pattern results of the Au-NPs/PPyC/$SrTiO_3$ NCs. Lattice

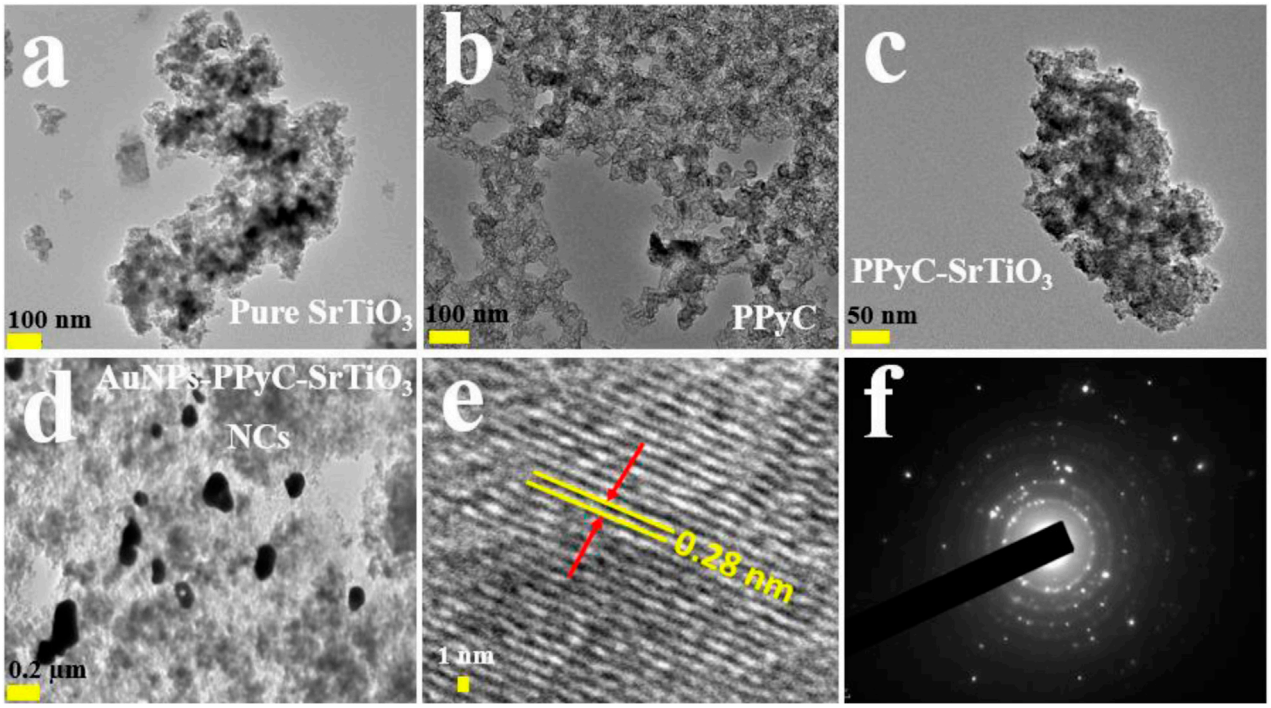

FIGURE 4
HRTEM analyses of the NCs. Magnified images of **(A)** pure $SrTiO_3$, **(B)** PPyC, **(C)** PPyC/$SrTiO_3$, and **(D)** Au-NPs/PPyC/$SrTiO_3$ NCs; **(E)** lattice spacing and **(F)** selected-area electron diffraction pattern of the NC.

fringes/spacing are visible in the HRTEM image of the Au-NPs/PPyC/$SrTiO_3$ NC in Figure 4E, suggesting that the nanocrystal structure is well-ordered and devoid of displacements. Further evidence that the NC is crystalline was found when the d-spacing between lines in the lattice was determined to be 0.28 nm. In Figure 4F, we see the selected area electron diffraction (SAED) results of the probed Au-NPs/PPyC/$SrTiO_3$ NC, which exhibits bright spots grouped in a concentric pattern, confirming the crystalline character of the ternary NC.

XPS analysis of the Au-NPs/PPyC/$SrTiO_3$ NC

Utilizing the XPS method, it is feasible to ascertain the oxidation states of the atoms in the NC. In this study, the XPS data of the synthesized Au-NPs/PPyC/$SrTiO_3$ NCs were analyzed to gather valuable information regarding the chemical composition and oxidation states of the NC. As presented in Figure 5A, the Ti2p orbital was subdivided into two spin orbitals, $Ti2p_{3/2}$ and $Ti2p_{1/2}$, indicating Ti^{4+} ionization (Nawaz et al., 2019; Faisal et al., 2023b). The Au-NPs exhibited XPS peaks at binding energies of 84 and 88 eV for the $4f_{7/2}$ and $4f_{5/2}$ transitions, respectively, confirming the presence of Au-NPs in the NC, as shown in Figure 5B (Vitale et al., 2011; Chen et al., 2015). Figure 5C presents two peaks at 270 and 280.5 eV for $Sr3d_{5/2}$ and $Sr3d_{3/2}$, respectively, confirming the existence of Sr^{2+} in the prepared NCs (Atuchin et al., 2013; Li et al., 2017). The O1s orbital shown in Figure 5D displays a peak at 531 eV for Ti-O or Sr-O, confirming the oxidation state of Ti(II) (Bakhoum et al., 2022). The C1s XPS curve shown in Figure 5E represents the C-O bond (Xiao et al., 2017; Bourlier et al., 2018) while the N1s orbital in Figure 5F shows C=N and O-N peaks (Majumdar et al., 2012; Ravi et al., 2018). Overall, the XPS analysis confirmed the existence of Sr^{+2}, Ti^{4+}, Au-NPs, and O^{2+} as well as C-O, C=N, and O-N bonds in the synthesized NCs, providing valuable information regarding their chemical compositions and oxidation states.

Crystallographic, optical absorbance, and surface area analyses

The crystallographic study of the prepared NC was conducted via powder dispersion using X-rays, as shown in Figure 6A. The obtained data clearly indicate that the crystalline peaks of the synthesized Au-NPs/PPyC/$SrTiO_3$ NC are SrO and TiO_2 only. The crystallographic study revealed peaks for TiO_2 corresponding to the (211) and (116) planes (Fang et al., 2012; Kaygili et al., 2017; Fu et al., 2023). Several crystalline peaks of SrO were also detected, corresponding to the (110), (121), and (200) planes, in accordance with a previous report (Tan et al., 2014; Tabah et al., 2017; Trang et al., 2021; Cai et al., 2023). Additionally, the XRD pattern for the prepared Au-NPs/PPyC/$SrTiO_3$ NC showed two extra peaks at 38.12 and 64.38 eV for the (1 1 1) and (2 2 0) crystal planes compared to the PPyC/$SrTiO_3$ sample, signifying the existence of Au NPs (JCPDS Card No. 01–1174). Finally, it is important to note that no contaminant peaks of any impurities were observed in the XRD investigations, confirming the formation of Au-NPs/PPyC/

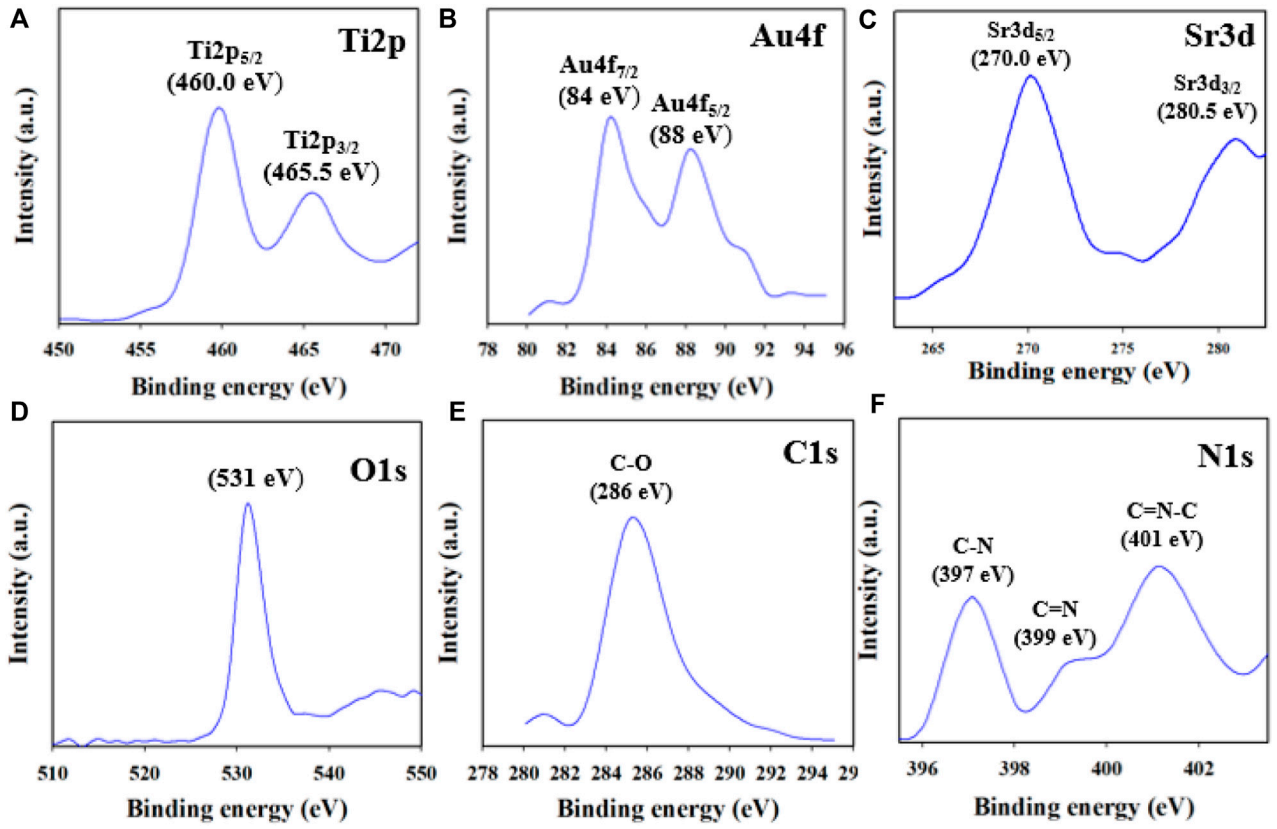

FIGURE 5
XPS results of the Au-NPs/PPyC/$SrTiO_3$ NC: **(A)** Ti2p, **(B)** Au4f, **(C)** Sr3d, **(D)** O1s, **(E)** C1s, and **(F)** N1s.

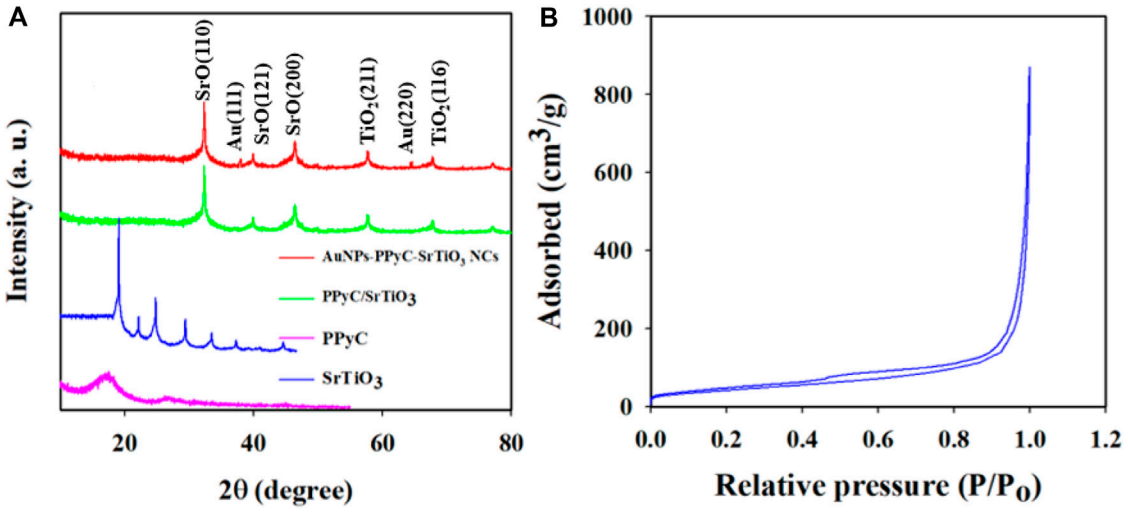

FIGURE 6
(A) Phase crystallinity analysis of the Au-NPs/PPyC/$SrTiO_3$ NC with comparison of its constituent elements and **(B)** surface area of the NC by BET analysis.

$SrTiO_3$ NCs only (Faisal et al., 2023a; Zhao et al., 2024). The obtained XRD values suggest the development of a structure containing Au-NPs, SrO, and TiO_2. The BET surface analysis was used to determine the active surface areas of the NCs using nitrogen adsorption and desorption, as demonstrated in Figure 6B. The calculated relative surface area of the Au-NPs/PPyC/$SrTiO_3$ NC is 119.34 m^2/g, indicating that the NC exhibits a good surface area favorable for electrocatalytic

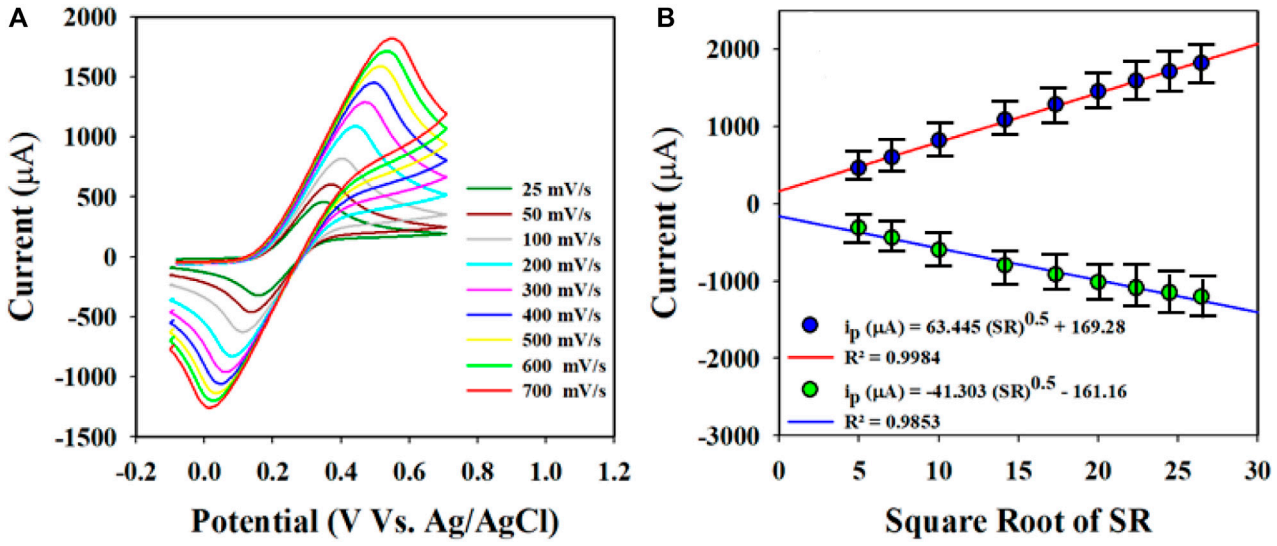

FIGURE 7
Electrochemical characterization of the Au-NPs/PPyC/$SrTiO_3$ NC using cyclic voltammetry (CV): **(A)** investigation of the scan rate of the coated GCE using Au-NPs/PPyC/$SrTiO_3$ NC in the oxidation reduction of 0.1 mM $K_4[Fe(CN)_6]$; **(B)** peak current *versus* square root of the SR for nitrite detection by CV with the Au-NPs/PPyC/$SrTiO_3$ NC/GCE probe.

reactions. The pore size and pore volume (BJH results) of the Au-NPs/PPyC/$SrTiO_3$ NCs were found to be 16.61 nm and 0.65 cm^3/g, respectively.

Electrochemical characterization of the Au-NPs/PPyC/$SrTiO_3$ NC/GCE probe

CV measurements were obtained at a scan rate of 25–700 mV/s to assess the molecular diffusional ability on the WE surface (Au-NPs/PPyC/$SrTiO_3$ NC/GCE) using the PBS phase at pH 7.0 containing 0.1 mM K_4 $[Fe(CN)_6]$, as presented in Figure 7A. Figure 7A displays a linear distribution of the peak currents measured during the oxidation/reduction of K_4 $[Fe(CN)_6]$. Therefore, good electrochemical performance of the modified electrode for detecting electroactive species is revealed in the current *versus* square root of the scan rate (SR) plot, as shown in Figure 7B. The equations (Equations 1, 2) representing the plot are also given.

$$i_p = 63.445\ (SR)^{0.5} + 169.28;\ R^2 = 0.9984 \text{ at oxidation of } K_4[Fe(CN)_6] \quad (1)$$

$$ip = -41.303\,(SR)^{0.5} - 161.16;\ R^2 = 0.9853 \text{ at reduction of } K_4[Fe(CN)_6] \quad (2)$$

These equations indicate that the molecules are controlled by diffusion on the fabricated WE surface, as similar phenomena have been reported previously (Alam et al., 2022; Rahman et al., 2022; Faisal et al., 2023d; Li J. et al., 2023; Rahman et al., 2023). Nitrite was analyzed using the CV electrochemical method in a pH 7.0 conductive buffer solution, as presented in Figure 8A. The nitrite oxidation peak currents are shown to scale linearly with concentrations from 150.0 to 1500.0 μM. As shown in Figure 8B, the dispersed currents increase from 150.0 to 1500.0 μM, and this concentration range is determined to be the LDR for nitrite detection. The current vs. concentration plot is expressed by Equation 3 below:

$$i_p = 0.0158\,C(\mu M) + 8.6014;\ R^2 = 0.9879 \text{ at Oxidation of Nitrite} \quad (3)$$

The built-in nitrite sensor's sensitivity was determined using the slope of its calibration curve, and the best sensitivity for detecting nitrite was 0.5 μA/μM•cm^2. The LOD was determined to be 18.99 ± 0.95 μM for the nitrite sensor, and the LOD was calculated from the equation LOD = 3.3σ/S, where σ and S refer to the standard deviation of the blank responses and slope of the calibration curve, respectively.

Optimization of the Au-NPs/PPyC/$SrTiO_3$ NC/GCE sensor probe

In this approach, the WEs were fabricated using various compositions of the prepared target Au-NPs/PPyC/$SrTiO_3$ NC, including the bare GCE, $SrTiO_3$, and PPyC/$SrTiO_3$, as presented in Figure 9. It is shown that the Au-NPs/PPyC/$SrTiO_3$ NC/PEDOT:PSS/GCE exhibits the maximum oxidation current compared to the other constituent compositions in a pH 7.0 buffer containing 750 μM of nitrite using CV analysis. The pH of the buffer is a significant factor in the detection of nitrite compounds under identical conditions. Therefore, the oxidation performance of nitrite was also tested in a wide pH range (from acidic to basic; 5.5–8.0), as presented in Figures 9B, C. These results clearly demonstrate that efficient oxidation in the buffer containing 750.0 μM nitrite was obtained at pH 7.0 with the Au-NPs/PPyC/$SrTiO_3$ NC/PEDOT:PSS/GCE probe through the CV technique, indicating that the chemical sensor probe has good selectivity and sensitivity for nitrite detection at physiological pH values.

Stable performance of the WE in an electrochemical reaction is a key characteristic for measuring reliability. The glassy carbon WE

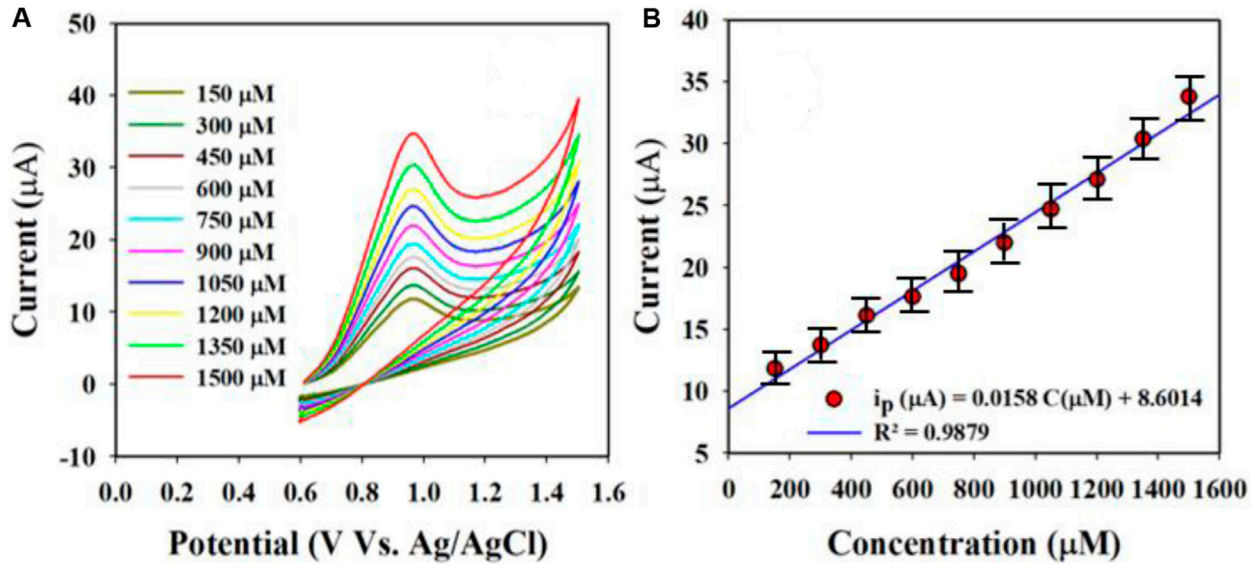

FIGURE 8
Nitrite is evaluated electrochemically through differential pulse voltammetry (DPV): **(A)** oxidation peak currents increased with concentration and **(B)** calibration curves of the nitrite sensor (current vs. concentration).

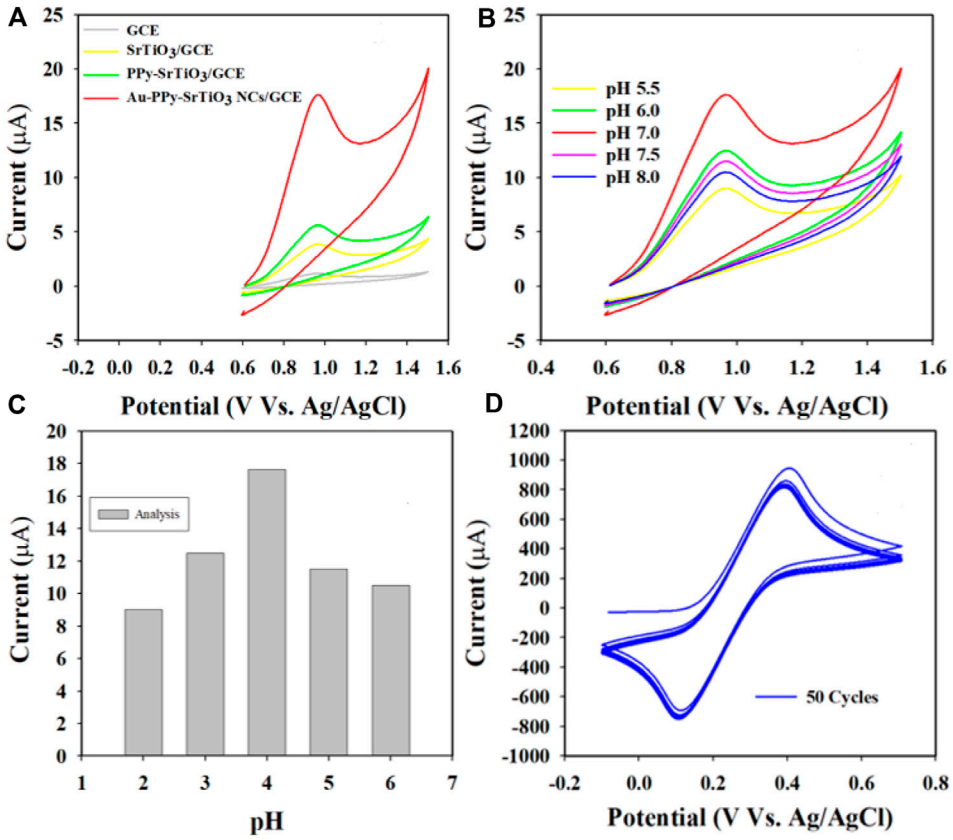

FIGURE 9
pH optimization in nitrite detection with the Au-NPs/PPyC/$SrTiO_3$ NC/PEDOT:PSS fabricated GCE probe: **(A)** controlled experiment, **(B)** CV analysis of nitrite based on pH of the buffer, **(C)** bar diagram, and **(D)** stability performance of the working electrode.

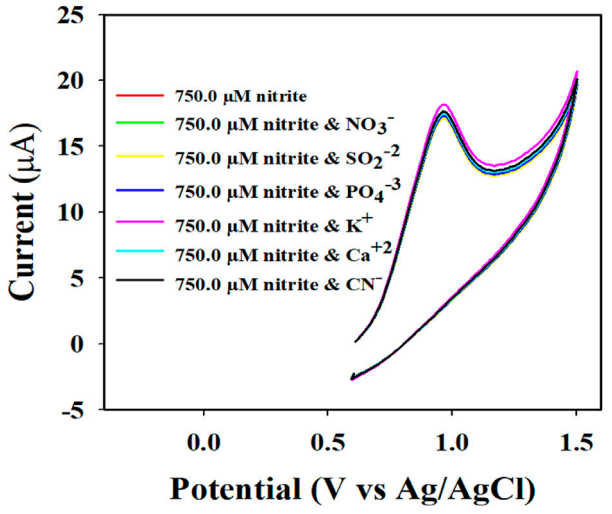

FIGURE 10
Electrochemical investigation of 750.0 μM nitrite in the presence of other analytes by the CV technique.

coated with Au-NPs/PPyC/$SrTiO_3$ NC was examined in the analysis of 0.1 mM K_4 [$Fe(CN)_6$], as shown in Figure 9D. As presented, the 50 cycles of CV were almost indistinguishable, meaning that the working electrode was active, which indicates the high stability of the WE prepared with Au-NPs/PPyC/$SrTiO_3$ NCs; this probe is expected to exhibit similar performances in other analytes.

To investigate the nitrite electrochemical sensor based on Au-NPs/PPyC/$SrTiO_3$ NC/PEDOT:PSS/GCE, interference was performed with a 750.0 μM nitrite solution in the presence of other ions, whose results are presented in Figure 10. The results are further analyzed and explored in Figure 10, where it is clearly illustrated that the nitrite electrochemical sensor did not show any interference in the presence of other ions such as NO_3^-, SO_2^{-2}, PO_4^{-3}, K^+, Ca^{+2}, and CN^-. Thus, the Au-NPs/PPyC/$SrTiO_3$ NC/PEDOT:PSS/GCE electrochemical sensor probe is selective toward only nitrites under identical conditions.

To validate the results of this electrochemical sensor study, comparisons were performed with similar studies using different sensing substrates, as shown in Table 1 (Zhang et al., 2013; Ma et al., 2014; Singh et al., 2019; Asiri et al., 2020; Rashed et al., 2020; Manikandan et al., 2021; Faisal et al., 2023c). From Table 1, it is seen that the Au-NPs/PPyC/$SrTiO_3$ NC/PEDOT:PSS/GCE sensor provides better results than other modified electrodes, with reliable parameters in terms of the sensitivity, LDR, and LOD.

Detection of nitrites with the Au-NPs/PPyC/$SrTiO_3$ NC/GCE probe

The detection mechanism for nitrite (NO_2^-) is illustrated in Scheme 1. Initially, H_2O molecules are adsorbed onto the Au-NPs/PPyC/$SrTiO_3$ NC/PEDOT:PSS/GCE probe surface, leading to electrocatalytic oxidation reaction and formation of H^+ and O^- ions. In the second stage, the NO_2^- ions react with O^- ions and are oxidized to nitrate (NO_3^-) ions, generating free electrons on the Au-NPs/PPyC/$SrTiO_3$ NC surface. This process leads to a significant increase in the conductivity of the fabricated electrode in the PBS phase, as shown in the reactions of Schemes 1A, B. The oxidation of nitrite to nitrate along with the production of electrons is a typical electrochemical reaction, and similar electrochemical oxidation reactions of nitrite (NO_2^-) have been reported elsewhere (Asiri et al., 2020; Rashed et al., 2020; Faisal et al., 2023c; Suiyi et al., 2024). The proposed detection mechanism highlights the efficient catalytic activity of the prepared Au-NPs/PPyC/$SrTiO_3$ NC/GCE probe toward nitrite detection, providing valuable insights into the electrochemical processes involved (Equations 4–6) in the detection of nitrite using the MC (Zhang et al., 2013; Zhu et al., 2017; Fu et al., 2020; Rashed et al., 2020).

$$NaNO_2 \rightarrow Na^+ + NO_2^- \quad (4)$$

$$H_2O \rightarrow 2H^+ + O^- \quad (5)$$

$$NO_2^- + O^- \rightarrow NO_3^- + e^- \quad (6)$$

Real sample analysis the with Au-NPs/PPyC/$SrTiO_3$ NC/GCE probe

In the final step to validate the sensor for the proposed applications, the prepared Au-NPs/PPyC/$SrTiO_3$ NC/PEDOT:PSS/GCE probe was used to measure various real samples collected from the environment, as listed in Table 2. The electrochemical analysis involved using the recovery technique and an electrochemical approach. Figure 8B shows a calibration curve for the desired

TABLE 1 Comparative analysis of the nitrite sensor probe based on different sensing substrates via the electrochemical technique.

Electrode materials	LOD	LDR	Sensitivity	Ref.
AuNPs/GO	6.00 nM	0.02~0.153 μM	---	Singh et al. (2019)
Au-G-PANI/GCE	0.01 μM	0.1~200 μM	---	Ma et al. (2014)
Au/Co_3O_4/GCE	0.11 μM	1.0~4,000.0 μM	---	Manikandan et al. (2021)
Cu-NDs/RGO/GCE	0.4 μM	1.25 μM to 13 mM	2.14 μA/$mM^{-1}cm^2$	Zhang et al. (2013)
rGO/ZnO/GCE	1.18 μM	20~520 μM	0.32 μA/$\mu M^{-1}cm^2$	Rashed et al. (2020)
GS/MWCNT/CD	1.65 μM	5 μM to 6.75 mM	---	Zhang et al. (2011)
Au@PPy-C/C_3N_4 NCs/GCE	1.11 ± 0.05 μM	1.5~22.5 μM	91.2 μA/$\mu M^{-1}cm^2$	Faisal et al. (2023c)
La_2CuO_4/Naf/GCE	0.04 μM	0.1–480 μM	12.0 μA/$\mu M^{-1}cm^2$	Asiri et al. (2020)
Au-NPs/PPyC/$SrTiO_3$ NCs/PEDOT:PSS/GCE	18.99 μM	150~1,500 μM	500.0 nA/$\mu M^{-1}cm^2$	*This study*

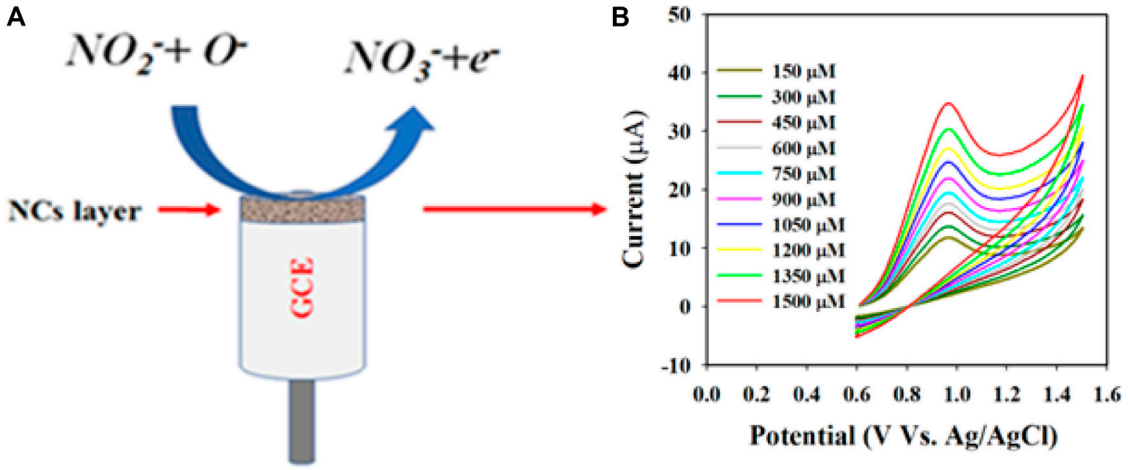

SCHEME 1
Schematic representation of the detection mechanism of nitrite with the Au-NPs/PPyC/$SrTiO_3$ NC/PEDOT:PSS fabricated GCE: **(A)** electrochemical oxidation of nitrite (NO_2^-) on the fabricated electrode and **(B)** conversion of NO_2^- to NO_3^- depending on the injected concentration in the electrochemical cell.

TABLE 2 Recovery approach applied to the analyses of real samples using a sensor probe made of Au-NPs/PPyC/$SrTiO_3$ NC/PEDOT:PSS/GCE.

Real sample	Added nitrite conc. (µM)	Measured nitrite Conc.[a] by the Au-NPs/PPyC/$SrTiO_3$ NC (µM)			Average recovery[b] (%)	RSD[c] (%) (n = 3)
		R1	R2	R3		
Underground water	750	742	745	743	99.11	0.205
Sea water	750	755	748	753	100.26	0.479
Tap water	750	739	740	755	99.20	1.204

[a]Calculations using the Au-NPs/PPyC/$SrTiO_3$ NC/GCE were averaged across three repetitions (signal-to-noise ratio = 3).
[b]Measurement or calculation of nitrite concentration. (Unit: µM).
[c]Accuracy from three replicated measurements (R_1, R_2, and R_3) is represented by the relative standard deviation (RSD) value.

nitrite concentration. The obtained results are presented in Table 2, indicating successful detection of nitrites in different real samples from the environment using the Au-NPs/PPyC/$SrTiO_3$ NC/PEDOT:PSS/GCE probe and electrochemical method. The sensor was found to be reliable and satisfactory, which indicates its potential for various environmental monitoring applications. Thus, the fabricated sensor with Au-NPs/PPyC/$SrTiO_3$ NC/PEDOT:PSS/GCE can be implemented in microsized electrochemical electrodes/devices for *in situ* usage to allow continuous measurement of nitrite ions in various environmental samples via the electrochemical approach.

Conclusion

In this study, Au-NPs-conjugated PPyC/$SrTiO_3$ NCs were deposited on GCEs to develop efficient nitrite electrochemical sensors with more conductive sensor-substrate using PEDOT:PSS as a conducting binder. The Au-NPs/PPyC/$SrTiO_3$ NCs were initially synthesized through ultrasonication, followed by photoreduction, resulting in a morphology that promotes electrochemical reactions for detecting nitrites under ambient conditions via the three-electrode system. The Au-NPs/PPyC/$SrTiO_3$ NC/PEDOT:PSS/GCE sensor probe exhibits high sensitivity, high LOD, and large LDR, indicating its potential for various environmental monitoring applications. To validate its practical application, the Au-NPs/PPyC/$SrTiO_3$ NC/PEDOT:PSS/GCE probe was directly tested on real environmental samples, and satisfactory performance was observed with the electrochemical technique through the recovery approach. This electrochemical nitrite sensor probe, which uses a novel NC material, provides an easy-to-use tool for detecting nitrite levels and has significant potential for environmental and healthcare applications. The present study therefore provides valuable insights into the development of efficient and reliable sensors for environmental monitoring, facilitating real-time detection and quantification of nitrite levels in various environmental samples.

Data availability statement

The original contributions presented in the study are included in the article/Supplementary Material, and any further inquiries may be directed to the corresponding authors.

Author contributions

MF: Formal analysis, Funding acquisition, Investigation, Methodology, Writing–review and editing. MA: Formal analysis, Investigation, Methodology, Writing–original draft. JAh: Formal analysis, Investigation, Methodology, Writing–review and editing. AA: Formal analysis, Investigation, Methodology, Resources, Writing–review and editing. JA: Formal analysis, Investigation, Resources, Writing–review and editing. RA: Formal analysis, Funding acquisition, Investigation, Methodology, Writing–review and editing. FH: Formal analysis, Funding acquisition, Methodology, Resources, Writing–review and editing. MR: Conceptualization, Investigation, Supervision, Validation, Visualization, Writing–original draft.

Funding

The author(s) declare financial support was received for the research, authorship, and/or publication of this article. The authors are thankful to the Deanship of Graduate Studies and Scientific Research at Najran University for funding this work under the Growth Funding Program grant code (NU/GP/SERC/13/226-1).

Acknowledgments

The authors are thankful to the Deanship of Graduate Studies and Scientific Research at Najran University for funding this work under the Growth Funding Program grant code (NU/GP/SERC/13/226-1).

Conflict of interest

The authors declare that the research was conducted in the absence of any commercial or financial relationships that could be construed as a potential conflict of interest.

Publisher's note

References

Alam, M. M., Asiri, A. M., Hasnat, M. A., and Rahman, M. M. (2022). Detection of L-aspartic acid with Ag-doped ZnO nanosheets using differential pulse voltammetry. *Biosensors* 12, 379. doi:10.3390/bios12060379

Amini, N., Maleki, A., and Maleki, P. (2021). Electrochemical detection of nitrate ions via reduction of NO2– and oxidation of NO reactions based on Cu@TiO2 coreshell/nafion/polyalizarin immobilized electrode. *Mater. Chem. Phys.* 264, 124384. doi:10.1016/j.matchemphys.2021.124384

Asiri, A. M., Adeosun, W. A., and Rahman, M. M. (2020). Development of highly efficient non-enzymatic nitrite sensor using La_2CuO_4 nanoparticles. *Microchem. J.* 159, 105527. doi:10.1016/j.microc.2020.105527

Atuchin, V. V., Kesler, V. G., Zaitsev, A. I., Molokeev, M. S., Aleksandrovsky, A. S., Kuzubov, A. A., et al. (2013). Electronic structure of α-SrB_4O_7: experiment and theory. *J. Phys. Condens. Matter.* 25, 085503. doi:10.1088/0953-8984/25/8/085503

Bahadoran, Z., Mirmiran, P., Jeddi, S., Azizi, F., Ghasemi, A., and Hadaegh, F. (2016). Nitrate and nitrite content of vegetables, fruits, grains, legumes, dairy products, meats and processed meats. *J. Food Compos. Anal.* 51, 93–105. doi:10.1016/j.jfca.2016.06.006

Bakhoum, D. T., Oyedotun, K. O., Sarr, S., Sylla, N. F., Maphiri, V. M., Ndiaye, N. M., et al. (2022). A study of porous carbon structures derived from composite of cross-linked polymers and reduced graphene oxide for supercapacitor applications. *J. Energy Storage.* 51, 104476. doi:10.1016/j.est.2022.104476

Bartsch, H., Hietanen, E., and Malaveille, C. (1989). Carcinogenic nitrosamines: free radical aspects of their action. *Free Radic. Biol. Med.* 7 (6), 637–644. doi:10.1016/0891-5849(89)90144-5

Bedale, W., Sindelar, J. J., and Milkowski, A. L. (2016). Dietary nitrate and nitrite: benefits, risks, and evolving perceptions. *Meat Sci.* 120, 85–92. doi:10.1016/j.meatsci.2016.03.009

Booth, M. A., Harbison, S., and Travas-Sejdic, J. (2011). Development of an electrochemical polypyrrole-based DNA sensor and subsequent studies on the effects of probe and target length on performance. *Biosens. Bioelectron.* 28 (1), 362–367. doi:10.1016/j.bios.2011.07.051

Bourlier, Y., Bouttemy, M., Patard, O., Gamarra, P., Piotrowicz, S., Vigneron, J., et al. (2018). Investigation of InAlN layers surface reactivity after thermal annealings: a complete XPS study for HEMT. *ECS J. Solid State Sci. Technol.* 7 (6), P329–P338. doi:10.1149/2.0181806jss

Cai, X., Li, X., You, J., Yang, F., Shadike, Z., Qin, S., et al. (2023). Lithium-mediated ammonia electrosynthesis with ether-based electrolytes. *J. Am. Chem. Soc.* 145 (47), 25716–25725. doi:10.1021/jacs.3c08965

Chen, Y., Zhang, J., Gao, Y., Lee, J., Chen, H., and Yin, Y. (2015). Visual determination of aliphatic diamines based on host–guest recognition of calix[4]arene derivatives capped gold nanoparticles. *Biosens. Bioelectron.* 72, 306–312. doi:10.1016/j.bios.2015.04.036

Edwards, G. C., Thurtell, G. W., Kidd, G. E., Dias, G. M., and Wagner-Riddle, C. (2003). A diode laser-based gas monitor suitable for measurement of trace gas exchange using micrometeorological techniques. *Agric. For. Meteorol.* 115, 71–89. doi:10.1016/S0168-1923(02)00166-1

Faisal, M., Alam, M. M., Ahmed, J., Asiri, A. M., Algethami, J. S., Alkorbi, A. S., et al. (2023a). Electrochemical detection of nitrite (NO2) with PEDOT:PSS modified gold/PPy-C/carbon nitride nanocomposites by electrochemical approach. *J. Ind. Eng. Chem.* 121, 519–528. doi:10.1016/j.jiec.2023.02.007

Faisal, M., Alam, M. M., Ahmed, J., Asiri, A. M., Alsareii, S. A., Alruwais, R. S., et al. (2023b). Efficient electrochemical detection of L-lactic acid using platinum nanoparticle decorated Chitosan/ZnTiO3 nanocomposites. *J. Ind. Eng. Chem.* 118, 362–371. doi:10.1016/j.jiec.2022.11.021

Faisal, M., Alam, M. M., Asiri, A. M., Alsaiari, M., Alruwais, R. S., Jalalah, M., et al. (2023c). Detection of hydrogen peroxide with low-dimensional silver nanoparticle-decorated PPy-C/TiO2 nanocomposites by electrochemical approach. *J. Electroanal. Chem.* 928, 117030. doi:10.1016/j.jelechem.2022.117030

Faisal, M., Algethami, J. S., Alorabi, A. Q., Ahmed, J., and Harraz, F. A. (2023d). Au nanoparticles dispersed polypyrrole-carbon black/SrTiO3 nanocomposite photocatalyst with rapid and stable photocatalytic performance. *J. Saudi Chem. Soc.* 27, 101741. doi:10.1016/j.jscs.2023.101741

Faisal, M., Rashed, M. A., Ahmed, J., Alhmami, M. A. M., Khan, M. K. A., Jalalah, M., et al. (2022). Pt nanoparticles decorated chitosan/ZnTiO3: ternary visible-light photocatalyst for ultrafast treatment of insecticide imidacloprid and methylene blue. *J. Taiwan Inst. Chem. Eng.* 133, 104266. doi:10.1016/j.jtice.2022.104266

Fang, J., Cao, S., Wang, Z., Shahjamali, M., Loo, S., Barber, J., et al. (2012). Mesoporous plasmonic Au-TiO2 nanocomposites for efficient visible-light-driven photocatalytic water reduction. *Int. J. Hydrog. Energy* 37, 17853–17861. doi:10.1016/j.ijhydene.2012.09.023

Fu, S., Wu, H., He, W., Li, Q., Shan, C., Wang, J., et al. (2023). Conversion of dielectric surface effect into volume effect for high output energy. *Adv. Mater.* 35 (40), 2302954. doi:10.1002/adma.202302954

Fu, Z. H., Yang, B. J., Shan, M. L., Li, T., Zhu, Z. Y., Ma, C. P., et al. (2020). Hydrogen embrittlement behavior of SUS301L-MT stainless steel laser-arc hybrid welded joint localized zones. *Corros. Sci.* 164, 108337. doi:10.1016/j.corsci.2019.108337

Griffiths, P. R., and De-Haseth, J. A. (2007). *Synthesis, properties, and applications of oxide nanomaterials*. Hoboken, New Jersey: John Wiley and Sons Inc.

Hamilton, J. F., and Lewis, A. C. (2006). in *Chromatographic methods*. Editor D. E. Heard (Hoboken, New Jersey: Blackwell Publishing), 361–405.

Hassan, M. H., Khan, R., and Andreescu, S. (2022). Advances in electrochemical detection methods for measuring contaminants of emerging concerns. *Electrochem. Sci. Adv.* 2, 2100184. doi:10.1002/elsa.202100184

Huang, Z., Luo, P., Wu, Q., and Zheng, H. (2022). Constructing one-dimensional mesoporous carbon nanofibers loaded with NaTi2(PO4)3 nanodots as novel anodes for

sodium energy storage. *J. Phys. Chem. Solids* 161, 110479. doi:10.1016/j.jpcs.2021.110479

Hussain, M., Hasnain, S., Khan, N. A., Bano, S., Zuhra, F., Ali, M., et al. (2021). Design and fabrication of a fast response resistive-type humidity sensor using polypyrrole (ppy) polymer thin film structures. *Polymers* 13, 3019. doi:10.3390/polym13183019

Kalaycıoğlu, Z., and Erim, F. B. (2019). Nitrate and nitrites in foods: worldwide regional distribution in view of their risks and benefits. *J. Agric. Food Chem.* 67 (26), 7205–7222. doi:10.1021/acs.jafc.9b01194

Kaminskay, O. V., Zakharov, E. A., and Slepchenko, G. B. (2004). Simultaneous voltammetric determination of nitrites and nitrates in waters. *J. Anal. Chem.* 59 (11), 1091–1096. doi:10.1023/B:JANC.0000047013.71862.c4

Kang, J., Liu, G., Hu, Q., Huang, Y., Liu, L., Dong, L., et al. (2023). Parallel nanosheet arrays for industrial oxygen production. *J. Am. Chem. Soc.* 145 (46), 25143–25149. doi:10.1021/jacs.3c05688

Karmakar, N., Fernandes, R., Jain, S., Patil, U. V., Shimpi, N. G., Bhat, N. V., et al. (2017). Room temperature NO2 gas sensing properties of p-toluenesulfonic acid doped silver-polypyrrole nanocomposite. *Sens. Actuator. B Chem.* 242, 118–126. doi:10.1016/j.snb.2016.11.039

Karwowska, M., and Kononiuk, A. (2020). Nitrates/nitrites in food—risk for nitrosative stress and benefits. *Antioxidants* 9, 241. doi:10.3390/antiox9030241

Kaygili, O., Bulut, N., Tatar, C., Ates, T., and İnce, T. (2017). Sol-gel synthesis and characterization of TiO2 powder. *Int. J. Innovative Eng. Appl.* 2, 38–40.

Kharat, H. J., Kakde, K. P., Savale, P. A., Datta, K., Ghosh, P., and Shirsat, M. D. (2007). Synthesis of polypyrrole films for the development of ammonia sensor. *Polym. Adv. Technol.* 18 (5), 397–402. doi:10.1002/pat.903

Li, J., Xu, J., Xu, M., Guan, T., Xia, Z., Jiang, L., et al. (2023). Synthesis of ZnTiO3/tourmaline/Ni foam catalyst and enhanced photocatalytic performance. *Arab. J. Chem.* 16, 104436. doi:10.1016/j.arabjc.2022.104436

Li, Q., Wang, H., Yu, H., Fu, M., Liu, W., Zhao, Q., et al. (2023). Engineering an ultrathin and hydrophobic composite zinc anode with 24 μm thickness for high-performance Zn batteries. *Adv. Funct. Mater.* 33 (40), 2303466. doi:10.1002/adfm.202303466

Li, X., Zhao, X., Huang, P., Wang, M., Huang, Y., Zhou, Y., et al. (2017). Enhanced electrochemical performance of SrF2-modified Li4Ti5O12 composite anode materials for lithium-ion batteries. *J. Alloys Compd.* 693, 61–69. doi:10.1016/j.jallcom.2016.09.089

Liu, B., Liu, X., Yuan, Z., Jiang, Y., Su, Y., Ma, J., et al. (2019). A flexible NO2 gas sensor based on polypyrrole/nitrogen-doped multiwall carbon nanotube operating at room temperature. *Sens. Actuator. B Chem.* 295, 86–92. doi:10.1016/j.snb.2019.05.065

Lu, G., Duan, L., Meng, S., Cai, P., Ding, S., and Wang, X. (2023). Development of a colorimetric and turn-on fluorescent probe with large Stokes shift for H2S detection and its multiple applications in environmental, food analysis and biological imaging. *Dyes Pigments* 220, 111687. doi:10.1016/j.dyepig.2023.111687

Ma, X., Miao, T., Zhu, W., Gao, X., Wang, C., Zhao, C., et al. (2014). Electrochemical detection of nitrite based on glassy carbon electrode modified with gold–polyaniline–graphene nanocomposites. *RSC Adv.* 4, 57842–57849. doi:10.1039/C4RA08543D

Majumdar, A., Das, S. C., Shripathi, T., and Hippler, R. (2012). Chemical synthesis and surface morphology of amorphous hydrogenated carbon nitride film deposited by N2/CH4 dielectric barrier discharge plasma. *Compos. Interfaces* 19, 161–170. doi:10.1080/15685543.2012.699751

Mane, A. T., Navale, S. T., Sen, S., Aswal, D. K., Gupta, S. K., and Patil, V. B. (2015). Nitrogen dioxide (NO2) sensing performance of p-polypyrrole/n-tungsten oxide hybrid nanocomposites at room temperature. *Org. Electron.* 16, 195–204. doi:10.1016/j.orgel.2014.10.045

Manikandan, V. S., Durairaj, S., Boateng, E., Sidhureddy, B., and Chen, A. (2021). Electrochemical detection of nitrite based on Co3O4-Au nanocomposites for food quality control. *J. Electrochem. Soc.* 168, 107505. doi:10.1149/1945-7111/ac2c14

Meng, D., Yamazaki, T., Shen, Y., Liu, Z., and Kikuta, T. (2009). Preparation of WO3 nanoparticles and application to NO2 sensor. *Appl. Surf. Sci.* 256, 1050–1053. doi:10.1016/j.apsusc.2009.05.075

Navale, S. T., Chougule, M. A., Patil, V. B., and Mane, A. T. (2014a). Highly sensitive, reproducible, selective and stable CSA-polypyrrole NO2 sensor. *Synth. Met.* 189, 111–118. doi:10.1016/j.synthmet.2014.01.005

Navale, S. T., Mane, A. T., Chougule, M. A., Sakhare, R. D., Nalage, S. R., and Patil, V. B. (2014b). Highly selective and sensitive room temperature NO2 gas sensor based on polypyrrole thin films. *Synth. Met.* 189, 94–99. doi:10.1016/j.synthmet.2014.01.002

Nawaz, R., Kait, C. F., Chia, H. Y., Isa, M. H., and Huei, L. W. (2019). Huei. Glycerol-mediated facile synthesis of colored titania nanoparticles for visible light photodegradation of phenolic compounds. *Nanomaterials* 9, 586. doi:10.3390/nano9111586

Nawrocki, J., and Andrzejewski, P. (2011). Nitrosamines and water. *J. Hazard. Mater.* 189 (1–2), 1–18. doi:10.1016/j.jhazmat.2011.02.005

Rahman, M. M., Alam, M. M., Asiri, A. M., Chowdhury, M. A., and Uddin, J. (2022). Electrocatalysis of 2,6-dinitrophenol based on wet-chemically synthesized PbO-ZnO microstructures. *Catalysts* 12 (7), 727. doi:10.3390/catal12070727

Rahman, M. M., Alam, M. M., Asiri, A. M., Chowdhury, S., and Alruwais, R. S. (2023). Sensitive detection of citric acid in real samples based on Nafion/ZnO-CuO nanocomposites modified glassy carbon electrode by electrochemical approach. *Mater. Chem. Phys.* 293, 126975. doi:10.1016/j.matchemphys.2022.126975

Rashed, M. A., Faisal, M., Harraz, F. A., Jalalah, M., Alsaiari, M., and Al-Assiri, M. S. (2020). rGO/ZnO/Nafion nanocomposite as highly sensitive and selective amperometric sensor for detecting nitrite ions (NO_2^-). *J. Taiwan Inst. Chem. Eng.* 112, 345–356. doi:10.1016/j.jtice.2020.05.015

Ravi, S., Zhang, S., Lee, Y. R., Kang, K. K., Kim, J. M., Ahn, J. W., et al. (2018). EDTA-functionalized KCC-1 and KIT-6 mesoporous silicas for Nd3+ ion recovery from aqueous solutions. *J. Ind. Eng. Chem.* 67, 210–218. doi:10.1016/j.jiec.2018.06.031

Singh, M., Kashyap, H., Singh, P. K., Mahata, S., Rai, V. K., and Rai, A. (2019). AuNPs/Neutral red-biofunctionalized graphene nanocomposite for nonenzymatic electrochemical detection of organophosphate via NO2 reduction. *Sens. Actuators B Chem.* 290, 195–202. doi:10.1016/j.snb.2019.03.131

Song, J., Wang, L., Qi, H., Qi, H., and Zhang, C. (2019). Highly selective electrochemical method for the detection of serotonin at carbon fiber microelectrode modified with gold nanoflowers and overoxidized polypyrrole. *Chin. Chem. Lett.* 30 (9), 1643–1646. doi:10.1016/j.cclet.2019.05.042

Suiyi, Z., Yanong, R., Yuxin, Z., Minglin, Z., Weilu, Y., Xinfeng, X., et al. (2024). A novel clinoatacamite route to effectively separate Cu for recycling Ca/Zn/Mn from hazardous smelting waterwork sludge. *J. Environ. Chem. Eng.* 12 (2), 112024. doi:10.1016/j.jece.2024.112024

Tabah, B., Nagvenkar, A. P., Perkas, N., and Gedanken, A. (2017). Solar-heated sustainable biodiesel production from waste cooking oil using a sonochemically deposited SrO catalyst on microporous activated carbon. *Energy fuels* 31, 6228–6239. doi:10.1021/acs.energyfuels.7b00932

Tamaki, J., Hayashi, A., Yamamoto, Y., and Matsuoka, M. (2003). Detection of dilute nitrogen dioxide and thickness effect of tungsten oxide thin film sensors. *Sens. Actuators B* 95, 111–115. doi:10.1016/S0925-4005(03)00417-9

Tan, H., Zhao, Z., Zhu, W. B., Coker, E. N., Li, B., Zheng, M., et al. (2014). Oxygen vacancy enhanced photocatalytic activity of perovskite $SrTiO_3$. *ACS Appl. Mater.* 6, 19184–19190. doi:10.1021/am5051907

Terbouche, A., Lameche, S., Terbouche, C. A. R., Guerniche, D., Lerari, D., Bachari, K., et al. (2016). A new electrochemical sensor based on carbon paste electrode/Ru(III) complex for determination of nitrite: electrochemical impedance and cyclic voltammetry measurements. *Measurement* 92, 524–533. doi:10.1016/j.measurement.2016.06.034

Tohidinia, M., Farsadrooh, M., Bahmanzadeh, S., Sabbaghi, N., and Noroozifar, M. (2018). Poly(quercetin)-bismuth nanowires as a new modifier for simultaneous voltammetric determination of dihydroxybenzene isomers and nitrite. *RSC Adv.* 8, 1237–1245. doi:10.1039/C7RA11132K

Trang, T. N. Q., Van, M. T., Phan, T. B., and Thu, V. T. H. (2021). Spatially controlled photogenerated charge carriers induced by $SrTiO_3$-architectured heterojunction nanocubes for a photocatalytic hydrogen evolution reaction. *ACS Appl. Energy Mater* 4, 8910–8921. doi:10.1021/acsaem.1c01163

Vitale, F., Fratoddi, I., Battocchio, C., Piscopiello, E., Tapfer, L., Russo, M. V., et al. (2011). Mono- and bi-functional arenethiols as surfactants for gold nanoparticles: synthesis and characterization. *Nanoscale Res. Lett.* 6, 103. doi:10.1186/1556-276X-6-103

Wang, C., Shi, P., Guo, C., Guo, R., and Qiu, J. (2024). CuCo2O4/CF cathode with bifunctional and dual reaction centers exhibits high RhB degradation in electro-Fenton systems. *J. Electroanal. Chem.* 956, 118072. doi:10.1016/j.jelechem.2024.118072

Wang, S., Liu, Y., He, L., Sun, Y., Huang, Q., Xu, S., et al. (2024). A gel polymer electrolyte based on IL@NH2-MIL-53 (Al) for high-performance all-solid-state lithium metal batteries. *Chin. J. Chem. Eng.* 69, 47–55. doi:10.1016/j.cjche.2024.01.017

Xiao, S., Xu, P., Peng, Q., Chen, J., Huang, J., Wang, F., et al. (2017). Layer-by-Layer assembly of polyelectrolyte multilayer onto PET fabric for highly tunable dyeing with water soluble dyestuffs. *Polymers* 9, 735. doi:10.3390/polym9120735

Zhang, D., Fang, Y., Miao, Z., Ma, M., Du, X., Takahashi, S., et al. (2013). Direct electrodeposion of reduced graphene oxide and dendritic copper nanoclusters on glassy carbon electrode for electrochemical detection of nitrite. *Electrochim. Acta* 107, 656–663. doi:10.1016/j.electacta.2013.06.015

Zhang, Y., Gao, H., Wang, J., Chi, Q., Zhang, T., Zhang, C., et al. (2024). PEO/Li1.25Al0.25Zr1.75(PO4)3 composite solid electrolytes for high-rate and ultra-stable all-solid-state lithium metal batteries with impregnated cathode modification. *Inorg. Chem. Front.* 11 (4), 1289–1300. doi:10.1039/D3QI02407E

Zhang, Y., Yuan, R., Chai, Y., Li, W., Zhong, X., and Zhong, H. (2011). Simultaneous voltammetric determination for DA, AA and NO2– based on graphene/poly-cyclodextrin/MWCNTs nanocomposite platform. *Biosens. Bioelectron.* 26 (9), 3977–3980. doi:10.1016/j.bios.2011.03.017

Zhao, X., Fan, B., Qiao, N., Soomro, R. A., Zhang, R., and Xu, B. (2024). Stabilized Ti3C2T -doped 3D vesicle polypyrrole coating for efficient protection toward copper in artificial seawater. *Appl. Surf. Sci.* 642, 158639. doi:10.1016/j.apsusc.2023.158639

Zhu, Q., Chen, J., Gou, G., Chen, H., and Li, P. (2017). Ameliorated longitudinal critically refracted—attenuation velocity method for welding residual stress measurement. *J. Mater. Process. Technol.* 246, 267–275. doi:10.1016/j.jmatprotec.2017.03.022